International Journal of Environmental Science and Technology (2024) 21:5165–5184
https://doi.org/10.1007/s13762-023-05347-0

ORIGINAL PAPER

Sodalite zeolitic materials produced from coal fly ash for removal of congo red dye from aqueous solutions

K. M. Abas[1] · **N. A. Fathy**[1]

Received: 18 April 2023 / Revised: 26 October 2023 / Accepted: 6 November 2023 / Published online: 25 November 2023

Abstract

Coal fly ash (CFA) is an excellent source of silica–alumina precursor that can be used for the copious and continuous manufacturing of zeolitic materials. This study provides a novel strategy to prepare zeolitic sodalite from CFA as adsorbents for Congo red (CR) dye removal under variable conditions. Sodalite crystals (S) were prepared by a calcination of sodium–aluminum silicate derived from CFA in either absence or presence of cetyltrimethylammonium bromide (CTAB) surfactant (CTAB-S). SEM, XRD, FTIR, and N_2 adsorption measurements were demonstrated. XRD results confirmed the presence of mullite and quartz as main components in CFA which converted to sodalite phases after calcination in existence of CTAB. SEM revealed that agglomerated larger particles were formed in S sample without adding CTAB, whereas smaller spherical particles aggregated together upon adding CTAB to form zeolitic structure (CTAB-S). FTIR showed the characteristic absorption bands of sodalite related to oxygen-containing Si and Al groups. Batch adsorption isotherm studies were conducted to evaluate the maximum adsorption capacities of S and CTAB-S, which were amounted to be 152.7 and 184.8 mg/g, respectively. Adsorption of CR dye was fitted with Freundlich isotherm. Kinetic results perfectly matched with pseudo-second-order model and intraparticle diffusion. Thermodynamic findings indicated that the adsorption of CR dye over both samples was endothermic and spontaneous in nature. CTAB-S sample showed the best reusable adsorbent, according to reuse experiments employing water as a desorbing agent. Overall, it can be concluded that CFA-derived sodalite can be used as an effective adsorbent for anionic dyes removal from wastewater.

Keywords Coal fly ash · Sodalite · Adsorption · Congo red dye

Introduction

Over 30 Mt of coal fly ash (CFA), as a by-product solid of coal combustion at power plants is produced annually in South Africa, with approximately 5% recovered for practical purposes from a global quantity of 800 Mt (Shumba et al. 2011). In the construction sector, CFA is widely applied as a supplement to concrete and cement. Also, it can be used to improve soil quality for agriculture, cover in low-lying areas, and create beneficial industrial catalysts (Shumba et al. 2011; Shabani et al. 2019). However, huge amount of CFA residues poses a significant environmental threat and thus causes adverse effects on land and in water (Musyoka et al. 2014). Naturally, CFA contains high ratios of glassy silicon and aluminum (alumina–silica material), which could reduce the production cost of zeolites to around one-fifth of that of commercial zeolites (Musyoka et al. 2014). Thus, CFA as feedstock for zeolite fabrication may not require multiple steps (Münzer et al. 2008).

As a type of zeolite, the sodalite phase gained much interests due to its accessible surface area, uniform pore structure, alkali resistance, and hydrothermal strength and thus it can serve as effective adsorbents and catalyst supports (Münzer et al. 2008; Nabavi et al. 2014; Günther et al. 2015; Golbad et al. 2017; Shabani et al. 2019). Sodalite can be obtained in a "b-cage" structure showing a framework with a cubic arrangement of SiO_4 and AlO_4 in four- and six-membered oxygen rings (Golbad et al. 2017). In recent years, the use of sodalite to purify

Editorial responsibility: A.Hanc.

✉ N. A. Fathy
fathyna.77@hotmail.com

[1] Physical Chemistry Department, Advanced Materials Technology and Mineral ResourcesResearch Institute, National Research Centre, 33 EL Buhouth St, P.O. 12622, Dokki, Cairo, Egypt

wastewater has attracted much interest. According to other investigations, the sodalite produced from CFA has exhibited an astonishing ability to remove cations like Pb^{2+} ions (154–157 mg/g) (Luo et al. 2016; Golbad et al. 2017).

However, the industrial production of sodalite remains a challenge due to the high cost of commercial reagents employed as feedstocks (Günther et al. 2015; Golbad et al. 2017; Shabani et al. 2019). Previous studies have been studied the hydrothermal process to prepare sodalite from CFA (Münzer et al. 2008; Nabavi et al. 2014; Günther et al. 2015; Golbad et al. 2017; Shabani et al. 2019). Therefore, the primary goal of this study was to fabricate zeolitic sodalite from CFA utilizing an easy and affordable process. The second goal was to investigate the viability of prepared sodalite adsorbents to clean aqueous solutions that have been polluted with dye solutions.

Due to the inherent poisonous, cancer and mutation effects of dyes, they present risks to both human health and biodiversity when exposed to aquatic environments (Vimonses et al. 2010). Congo red (CR) is the most prevalent anionic azo dye and is commonly found in the wastewater of the textile, paper, and printing industries. CR dye may be transformed into benzidine, a known human carcinogen and a potential contributor to allergic disorders in humans (Jiang et al. 2016). It has been reported that the adsorptive removal of CR dye from aqueous solutions using zeolitic imidazolate framework-8 (ZIF-8), that is a metal–organic framework (MOF) with a sodalite-network structure, was very excellent (Jiang et al. 2016; Cao et al. 2021). The adsorption capacity of CR onto ZIF-8 was extremely high at 1250 mg/g (Jiang et al. 2016) and 1340 mg/g (Cao et al. 2021) as a consequence of hydrophobic/electrostatic and π–π interactions between MOF and dye molecules. According to a later study, ZIF-67 as sodalite zeolitic MOFs may have an adsorption capacity for CR up to 714.3 mg/g (Thanh Tu et al. 2018). The capacity of CR dye on the bentonite/zeolite-NaP composite was investigated to be 46 mg/g, however; this adsorbent exhibited a large surface area of 512 m^2/g (Shaban et al. 2018). Nevertheless, there were no contribution studies made on CFA-derived sodalite to be used as adsorbent for the removal of the CR dye. Thereof, the present study was included the preparation crystalline sodalite zeolitic materials from CFA feedstock through direct calcination at 550 ℃ for 3 h in either absence or presence of a cationic surfactant called cetyltrimethylammonium bromide (CTAB). The stated procedure is assumed to be an available, eco-friendly, and simple to implement compared with other techniques used before to prepare CFA-derived sodalite (Nabavi et al. 2014; Günther et al. 2015; Golbad et al. 2017; Shabani et al. 2019). Relevant measurements such as SEM, XRD, FTIR, N_2 adsorption–desorption, as well as CR dye adsorption experiments (i.e., equilibrium, kinetic, and thermodynamic studies) from aqueous solutions were employed to assess the surface and adsorption properties of the prepared samples.

Materials and methods

Materials

Coal fly ash (CFA) was acquired as a by-product from an electrical power station, Spain. It consists of ~ 60.8% SiO_2, 29.9% Al_2O_3 and 3.80% Fe_2O_3 (Khattab et al. 2018). Cationic surfactant of cetyltrimethylammonium bromide (CTAB, C_{16} H_{33} $(CH_3)_3NBr$, Merck), sodium hydroxide pellets (NaOH, 98%, Modern-Lab), hydrochloric acid (HCl, 37%, Alpha-Chemika), ethanol (CH_3CH_2OH, 99%) and Congo red (CR) dye ($C_{32}H_{22}N_6Na_2O_6S_2$) were purchased from Sigma-Aldrich company.

Pretreatment of CFA for preparation of sodalite

In accordance with the described method by Aboelenin et al. (2017), CFA was pretreated with minor modifications to extract sodium–aluminum silicate. Briefly, 50 g of CFA particles with 3 N HCl solution in 250 mL of a conical flask were agitated for 15 min and then refluxed at 90 ℃ for 6 h, and subsequently immersed at room temperature for an 100 ℃ for additional 40 h to expel the remaining minerals. After that, the treated CFA was filtered and cleaned with ethanol and pre-heated distilled water until the pH was neutral. The resulting white solid was dried at 110 ℃ for 24 h. Then, the processed CFA was exposed to calcination at 700 ℃ for 3 h in a muffle furnace to remove organic components.

The calcined CFA used as a sodalite precursor was combined with 250 mL of a 3 N NaOH solution and refluxed at 100 ℃ for 2 h to create a suspended solution of the sodium–aluminum silicate. The established sodium–aluminum silicate solution was filtered through Whatman® filter paper No. 41. After allowing the viscous supernatant solution to settle to room temperature, two preparation routes were managed as follows (Kumar et al. 2001; Yadav and Fulekar 2019):

(a) 2 N HCl was used to lower the pH of the produced viscous supernatant to approximately 8 while stirring until gel formation. The produced gel was desiccated for 24 h at 150 ℃ in an air oven. After that, it was subjected to calcination at 550 ℃ for 3 h in an electrical muffle furnace. The aluminum–silicate substance (i.e., sodalite) was designated as "S."
(b) In the second route, about 1 g of CTAB dissolved in a small quantity of ethanol (70%), the viscous silicate supernatant was slowly spilled over the CTAB solution

(1% in accordance with the weight ratio of 1:100) while being stirred continuously for two hours. The generated solution was then modified to have a pH of 8 using 2 N HCl until gel development. The final product was then desiccated at 150 ℃ for 24 h in an air furnace; subsequently calcined at 550 ℃ for 3 h. The obtained sodalite was marked as "CTAB-S."

Characterization of prepared samples

Scanning electron microscope (SEM) of QUANTA FEG 250 ESEM (Japan) was used to analyze the morphology of the silicate-based materials. In addition, energy-dispersive X-ray spectroscopy (EDX) analysis at 20 kV voltage was used to record the compositions of prepared samples. A diffractometer (Bruker D8 Advance, Germany), namely X-ray diffraction (XRD) with Cu $K_{\alpha 1}$ ($\lambda = 0.15418$ nm) at room temperature was performed to characterize the prepared materials with monochromator settings at 40 kV and 40 mA. Fourier transform infrared (FT-IR) NICOLET 8700 spectrometer (Thermo Scientific, Loughborough, United Kingdom) through KBr pellets approach was employed to examine the particular functional surface groups of the obtained samples. N_2 adsorption–desorption isotherms obtained at − 196℃ by using Belsorp Microtrac BEL (Version 6.3.2.1) were analyzed to calculate the specific surface area (using the Brunauer–Emmett–Teller (BET) method) and the total pores generated in the prepared silicate-based materials.

Determination of point of zero charge

With addition of 0.1 N HCl and 0.1 N NaOH, the initial pH solutions (pH_i) values were regulated. In 100-mL flasks with 50 mL of the solution at different starting pH values (3, 4, 6, 8, and 10), and 0.25 g of silicate-based samples obtained from CFA, the experiments were carried out while being shaken for 24 h. The value of final pH (pH_f) of each supernatant was assessed after separation using a pH meter (HANNA® bench meter, HI111). The value of pH_{pzc} was calculated from the plateau of the pH_f versus pH_i curve.

Adsorption isotherms studies

Stock solutions were prepared by dissolving (20–200 mg) of CR dye in 1 L of distilled water at optimum conditions (pH 2 and 25 °C). In order to evaluate the impact of pH on the elimination of CR dye from aqueous solution, 100 mg of sodalite samples were conducted with 10 mL of CR dye (40 mg/L) at varied pHs (2, 4, and 6) and 25 ℃. Every sample was held in a rotating shaker at 220 rpm for 24 h at room temperature in order to reach equilibrium. The UV–visible absorption spectra of the supernatant solution were analyzed employing a UV–visible spectrophotometer (Type UV-2401PC) in a 1 cm quartz cuvette to check the characteristic absorption peaks of CR dye at a wavelength of 576 nm for pH of 2. The equilibrium adsorption amount, q_e (mg/g), was determined as stated to the following equation:

$$q_e = \frac{V(C_o - C_e)}{m} \tag{1}$$

where C_o and C_e (mg/L) are the initial and equilibrium concentrations in the liquid phase, V (mL) is the volume of the equilibrium solution, and m (mg) is the mass of the adsorbent. The following equation, in where R represents the removal efficiency of the CR dye, was used to establish the percentage of dye removal from the aqueous solution:

$$R(\%) = \frac{(C_o - C_e)}{C_o} \tag{2}$$

The Langmuir isotherm (Langmuir 1916; Foo and Hameed 2010) gauges the monolayer covering with symmetrical adsorption energies onto the homogeneous surface and no adsorbate evolution into the plate. It may be symbolized by the linear-form equation as shown below:

$$\frac{1}{q} = \frac{1}{K_L \cdot q_m}\left(\frac{1}{C_e}\right) + \frac{1}{q_m} \tag{3}$$

where C_e is the equilibrium dye concentration (mg/L), q_e denotes the equilibrium adsorption capacity (mg/g), q_m is the maximal adsorption capacity correlating to complete monolayer covering on the surface (mg/g), and K_L reflects the Langmuir constant (L/mg) signifying the manner of adsorption. The equilibrium parameter or separation factor of Langmuir (Weber and Chakravorti 1974) can be expressed by the following equation, R_L, which is the dimensionless constant for the highest initial concentration (C_o). This parameter declares as the fundamental characteristic of the Langmuir isotherm.

$$R_L = \frac{1}{1 + K_L \cdot C_o} \tag{4}$$

The adsorption property is indicated by the R_L value as being either unfavorable if $R_L > 1$, linear if $R_L = 1$, and favorable if $0 < R_L < 1$ and irreversible if $R_L = 0$ (Weber and Chakravorti 1974; Mohan and Chander 2001).

The Freundlich isotherm may be formulated as the following equation, and it offers an assessment of the adsorption characteristics for the heterogeneous surface (Freundlich 1906; Rangabhashiyam et al. 2014):

$$\log\ q_e = \log\ K_F + \frac{1}{n}\log C_e \tag{5}$$

where $K_F((mg/g)(L/mg)^{1/n})$ is the Freundlich isotherm constant, and n is the adsorption intensity constant. The

separation of the two phases at $n=1$ is concentration independent. If $1/n$ is less than 1, a typical adsorption is predicted. To the contrary hand, $1/n>1$ indicates a reciprocal adsorption (Delle Site 2001).

Adsorption dynamic study

Three kinetic famous models such as pseudo-first order, pseudo-second order, and intra-particle diffusion kinetic models were used to assess the CR adsorption mechanism onto sodalite specimens. To accomplish that, 1 g of prepared adsorbents was conducted to 100 mL of two different concentrations (40 and 120 mg/L) for the prepared CR dye solution at pH = 2 under continuous agitation. The correlation coefficients were used to represent how closely experimental data matched with values predicted by the model (R^2, values close or equal to 1). The model with the larger value is better appropriate for describing the kinetic of CR dye.

The first-order kinetic model

The adsorption rate constant was calculated from the first-order kinetic term (Lagergren 1898) given by Eq. (6):

$$\ln\left(q_e - q_t\right) = \ln\ q_e - K_1 t \tag{6}$$

where q_e and q_t (mg/g) are the quantity of dye that may be adsorbed per unit of weight at equilibrium and at time (t, min), respectively, and k_1 is the first order rate constant (min^{-1}). The plot of ln (q_e−q_t) against t was used to compute the first order kinetic parameters.

The second-order kinetic model

The second-order kinetic model (Ho and Chiang 2001) is termed as:

$$\frac{t}{q_t} = \frac{1}{K_2 q_e^2} + \frac{t}{q_e} \tag{7}$$

where the second-order rate constant, k_2 (g/mg.min), may be implemented analytically from the intercept of the line drawn by graphing (t/q_t) versus time (t, min).

Intra-particle diffusion study

The intra-particle diffusion mechanism is frequently the rate-limiting step in many adsorption processes especially in a rapid agitated batch reactor. This model reflects the migration of adsorbate species from the bulk of the solution into the solid surface. Weber–Morris plot (Weber and Morris 1963) explained that the adsorption changes exponentially with $t^{1/2}$ instead of the contact time (t) according to the equation:

$$q_t = K_{id} t^{\frac{1}{2}} + C \tag{8}$$

where k_{id} is the intra-particle diffusion rate constant (mg/g.$\text{min}^{1/2}$) estimated from the slope of a graph of (q_t) versus ($t^{1/2}$), and C is a constant calculated from the intercept when the adsorption mechanism follows the intra-particle diffusion process.

Adsorption thermodynamic study

Thermodynamic parameters such as standard enthalpy ($\Delta H°$, kJ/mol), standard free energy ($\Delta G°$, kJ/mol), and standard entropy ($\Delta S°$, J/mol.K) disclose details on the intrinsic energetic changes involved during the adsorption (Ahmad et al. 2014). To carry out this, 10 mL of CR dye (40 mg/L) and 100 mg of adsorbents under continuing agitation for 1 h at three temperatures (308, 318 and 328 K) were employed. The values of $\Delta H°$ and $\Delta S°$ are derived from applying Vant Hoff equation:

$$\ln\ K_L = \frac{\Delta S°}{R} - \frac{\Delta H°}{RT} \tag{9}$$

where R is the universal gas constant ($R=8.314$ J/mol.K), T is the absolute solution temperature (K), and K_L is the Langmuir isotherm constant (L/g). The $\Delta H°$ and $\Delta S°$ can be considered from the gradient and intercept, of (ln K_L) versus ($1/T$). Equation (10) can be used to gauge $\Delta G°$ value (Perrot 1998).

$$\Delta G° = \Delta H° - T \cdot \Delta S° \tag{10}$$

Results and discussion

SEM analysis

SEM images of pretreated CFA at 700 ℃ for 3 h and their sodalite specimens produced are displayed in Fig. 1. In general, the surface of pretreated CFA exhibited smooth spherical particles of diameter ranged from 2 to 8 µm of interposed and aggregated crystals. On the other hand, the as-synthesized sodalite-like (S) material exhibited accumulated and fractured tiny grains with low smooth surface and higher micrometer diameter as observed in (Fig. 1b). The increase in particle diameter and the lake of spherical particles in the treated CFA indicates a high alteration into more crystalline aluminum–silicate during

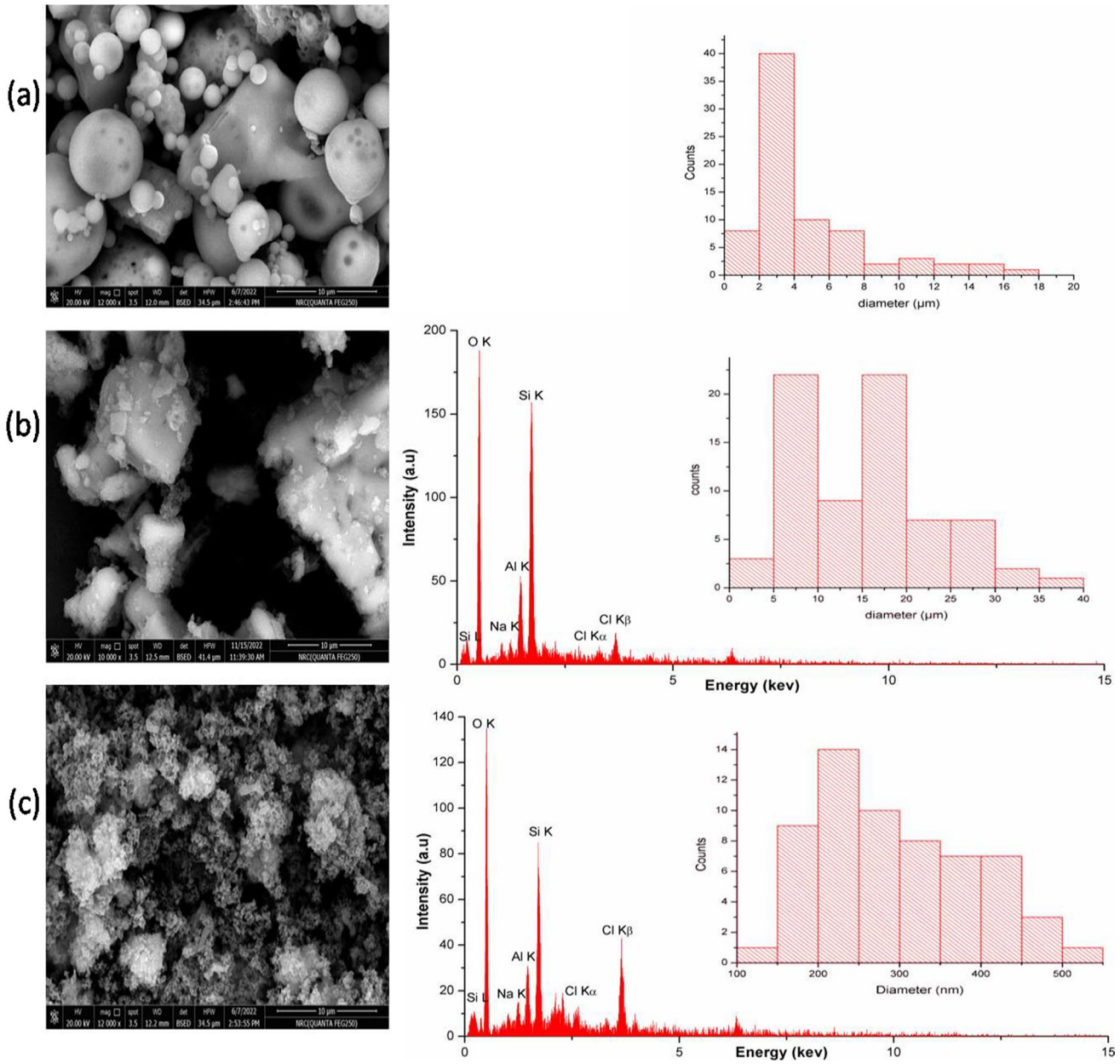

Fig. 1 SEM micrographs with histograms of diameter distribution of the prepared samples **a** CFA, **b** S and **c** CTAB-S and the corresponding EDX spectrum of both silicate samples

calcination of the treated CFA (Ojha et al. 2004). In the presence of CTAB surfactant, the calcination of CFA-derived silicate led to a considerable change in the surface, indicating the conversion of CFA to sodalite structure. As seen in Fig. 1c, the surface become rough and revealed a zeolitic-like crystals with diameters of 149–500 nm were deposited on the surface of CFA particles during the thermal treatment in presence of CTAB surfactant that could rapid the nucleation of aluminum–silicate particles to form zeolite-like clusters. Additionally, the particle size is getting smaller with CTAB because it reduces the tendency to aggregating of silicate particles (Purnawira et al. 2019). Therefore, the use of CTAB results in the formation of micelles structures, in turn inducing the bonds between silicate and prepared surfactants, and forming Si–O–H functional groups, whereas silicate-free CTAB particles contains Si–O–Si groups itself, which cause greater particle size as appeared in Fig. 1b (Zhao et al. 2013). EDX

analysis was accomplished for the CFA-based silicates in order to specify the elemental composition and inserted into Fig. 1. The spectra showed the characteristic peaks of Si, Al, and O with the presence of Na and Cl in a lower intensity which confirmed the chemical formula of sodalite as evidenced by XRD also.

XRD analysis

The X-ray diffraction patterns of CFA-derived silicates are shown in Fig. 2. The major crystalline materials of pretreated CFA are quartz (SiO_2, JCPDS CARD #46-1045), mullite ($Al_6Si_2O_{13}$, JCPDS CARD # 15-776), corundum (Al_2O_3, JCPDS CARD # 10-173) (Suriyana et al. 2009), and some traces of hematite (Fe_2O_3) appeared with lower intensity (Luo et al. 2016). In addition, Fig. 2 displays the crystallinity of S and CTAB-S, which is comparable to CFA with small hump at $2\theta = 20–25°$, verifying the presence of an amorphous silicon dioxide fraction and sodium silicate (Na_2SiO_3). Moreover, XRD diffraction patterns of S and CTAB-S samples revealed more than one crystalline phase. The predominant phase at $2\theta = 31.9°$ is corresponded to sodalite phase ($Na_8(Al_6Si_6O_{24})Cl_2$) according to JCPDS Card no (00-037-0196). In addition, XRD peak at $2\theta = 45.3°$ reflects the formation of quartz (SiO_2) (Bardez et al. 2008; Luo et al. 2016; Esaifan et al. 2019). It was found that the color of S and CTAB-S samples appeared as a reddish–brown and gray color, respectively. The appearance of reddish-brown color in S sample maybe owing to the presence of some iron cations (Ravikumar et al. 2005). Accordingly, employing CTAB surfactant could be reduced the quantity of iron oxides as evidenced by the appearance white color in CTAB-S sample. Nevertheless, on comparing the two prepared samples, it was observed that there are some differences in the peak intensity, indicating that the structure integrity of the sample is altered after surfactant treatment as accord with SEM results also (Singh et al. 2019).

FT-IR spectroscopy

The functional groups formed in the treated CFA and synthesized sodalite products were detected using FTIR tool. The results of their FTIR spectra are presented in Fig. 3. The asymmetrical stretching modes related to Si – O – Al groups that appeared at 1093 cm^{-1} for CFA was shifted to 1072 and 1068 cm^{-1} for S and CTAB-S, respectively; with increasing in their intensity (Makgabutlane et al. 2020). This finding was attributed to the formed highly crystalline silico-aluminates products which confirmed also by the XRD spectrum. Furthermore, two characteristic bands of zeolitic structure, centered at 795 and 450 cm^{-1}, were corresponded to vibrations of tetrahedral Si–O and Si–O–Al obtained in S and

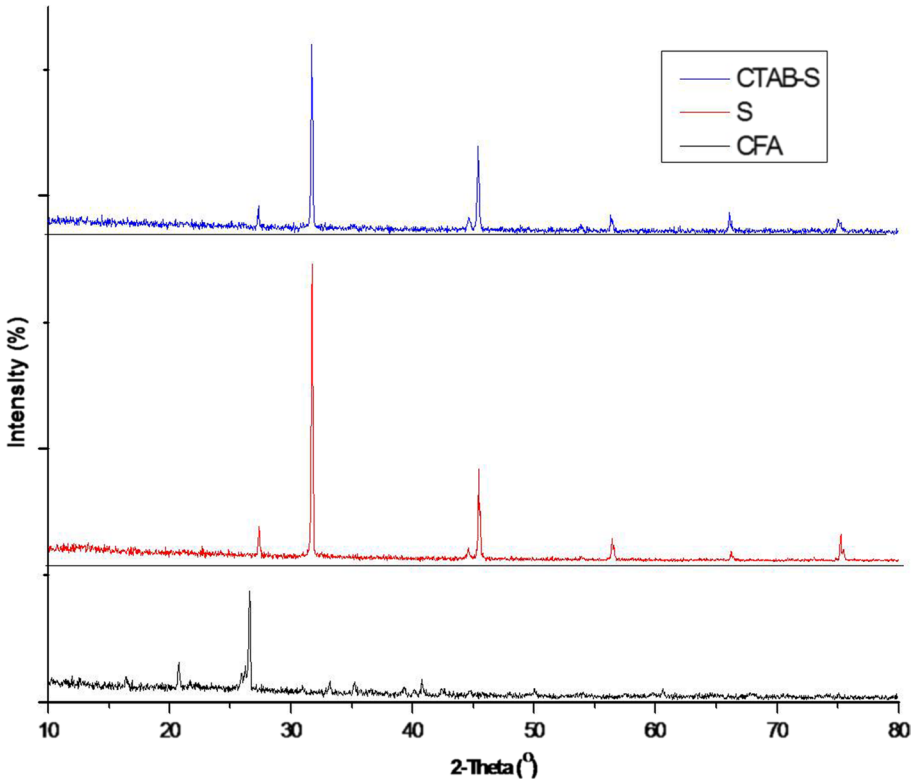

Fig. 2 XRD profile pattern of CFA-derived silicate samples

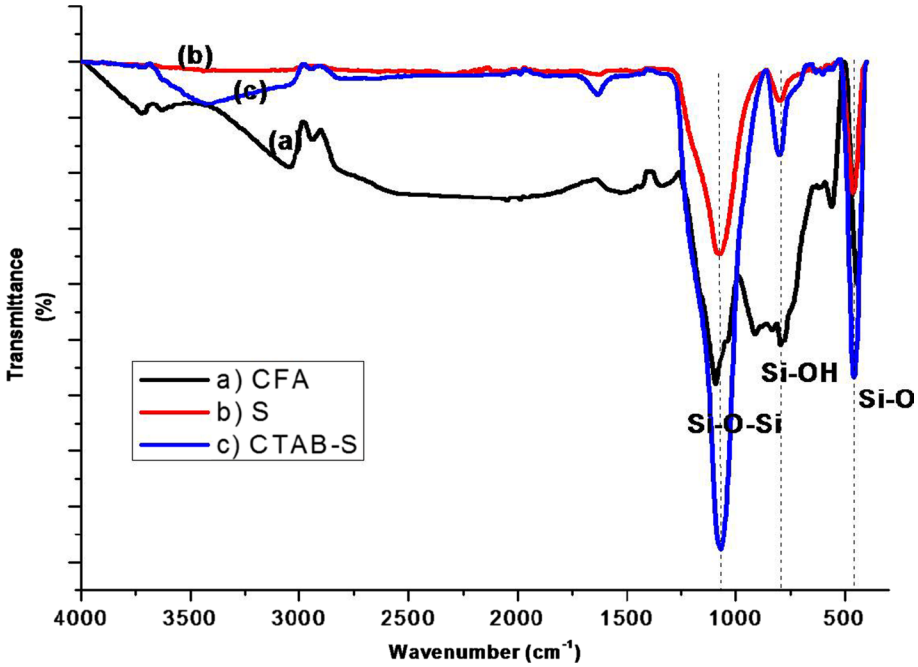

Fig. 3 FT-IR spectra of CFA-derived silicate samples

CTAB-S structures (Mucsi et al. 2014). In addition, bands between 450 and 500 cm^{-1} were related 450 and 500 cm^{-1} to an internal bending vibration of Si–O (Mucsi et al. 2014).

Shoulder bands appeared at around 3048–2940 cm^{-1} and 1530–1336 cm^{-1} in the sample of CFA were ascribed to the C–H and O–C = O stretching vibrations of the organic carbon, respectively (Alterary and Marei 2020). There was no peak at about 2800–3000 cm^{-1} for prepared S and CTAB-S samples which means that organic substances are removed after the calcination. Remarkably, two new vibrational bands observed at 3427 and 1631 cm^{-1} were due to O–H stretching and bending vibration of water molecules bound to the silicate matrix in the obtained CTAB-S structure (Mozgawa et al. 2014).

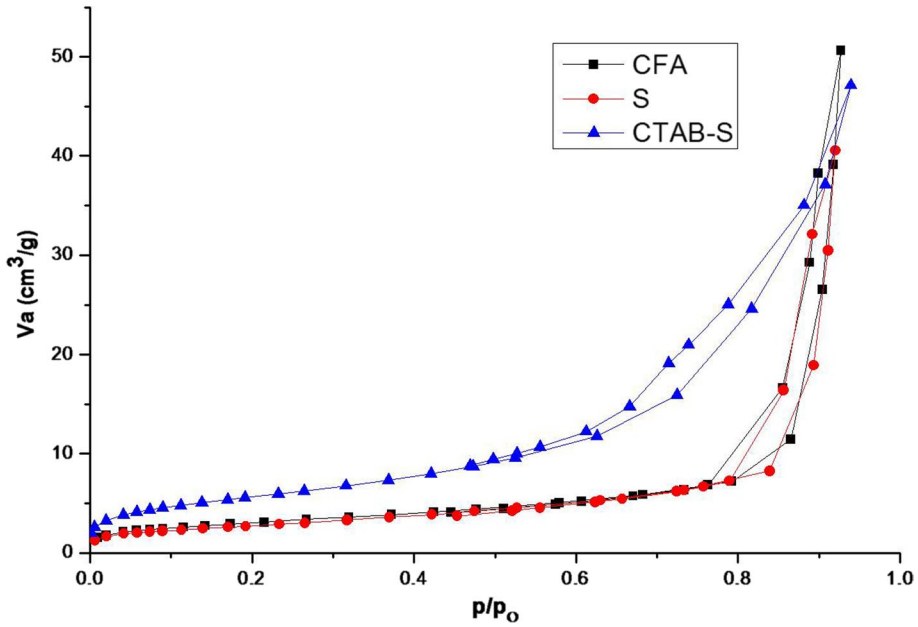

Fig. 4 N_2 adsorption–desorption measurements of prepared CFA-derived silicates

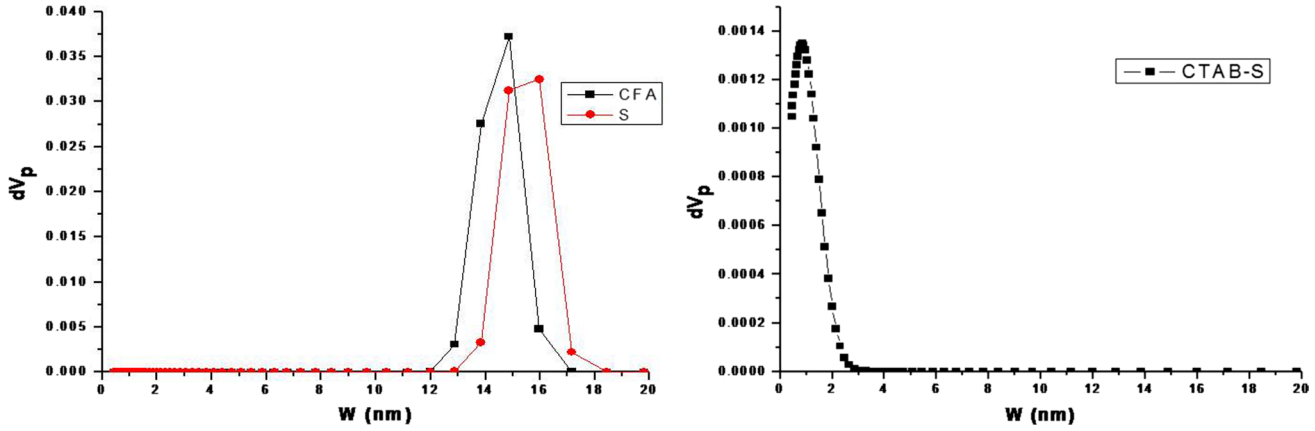

Fig. 5 NLDFT pore size distribution analysis of prepared CFA-derived silicates

Table 1 Surface area and PSD of prepared CFA-derived silicates

Specimens	S_{BET} (m^2/g)	Average pore diameter (nm)	V_{total} (cm^3/g)
CFA	11.2	28	0.08
S	10	25	0.06
CTAB-S	21	14	0.073

Surface textural analysis

The Brunauer–Emmett–Teller (BET) equation-based N_2 adsorption–desorption isotherms and its accompanied pore size distributions (PSDs) curve using non-local density functional theory (NLDFT) of all materials are depicted in Figs. 4 and 5, respectively. Their textural characteristics are counted in Table 1. The table shows that the CTAB-S has a specific surface area of 21 m^2/g, that is twice larger than CFA (11.2 m^2/g), and a total pore volume of 0.073 cm^3/g which less than that of CFA. The specific surface area of S (10 m^2/g) and total pore volume (0.06 cm^3/g) slightly declined less than those of the CFA sample (0.08 cm^3/g). It demonstrates that the surfactant treatment upgraded the surface area and reduced the average pore diameter of its produced silicate. The latter could be accounted for a rise in silicate micropores content as a result of the elimination of the organics through calcination posttreatment (Taufiq et al. 2018).

The N_2 adsorption–desorption profile (Fig. 4) reveals that the adsorption branch contains a low slope area associated with multilayer adsorption on pores, followed by pore condensation in mesopores, a plateau region shows fully filled mesopores at the end. The desorption branch pursues into hysteresis loops initiated at a high relative pressure $p/po > 0.76$ for CFA and its-derived S and S-CTAB samples. These characteristics indicate that the isotherms are of Type II with H1 hysteresis at a relative pressure $p/po > 0.5$ demonstrating the existence of mesopores (Sotomayor et al. 2018). These hysteresis loops are typically related to the capillary filling and condensation of N_2 inside the homogeneous slit-shaped mesopores produced by the accumulation of silicate crystals. The matching of PSDs further supported this (Ahmadpour and Taghizadeh 2015).

According to PSD profile (Fig. 5), the predominant pores in CTAB-S sample are virtually micropores that composed of narrow micropores with a width less than 2.0 nm. (Amani et al. 2018). This result confirms that the produced CTAB-S is a sodalite sample as shown in SEM section. On the other hand, PSDs of CFA and S showed pores with widths between 12 and 18 nm that are mesopores giving Type II *isotherm features.*

Surface characteristics of prepared CFA-based adsorbents

In addition to surface area and porosity, the adsorption characteristics of CFA, S, and CTAB-S may be influenced by the chemical composition of the surface. Consequently, the pH of point of zero charge (pH_{pzc}) of the produced adsorbents may offer an indicator to know the surface charges present on the prepared adsorbents. Such surface charges are formed as a result of the interaction between the adsorbent surface and the aqueous solution. The adsorbent surface is typically categorized into acidic, basic, and neutral (El-Sherif and Fathy 2013). Results of

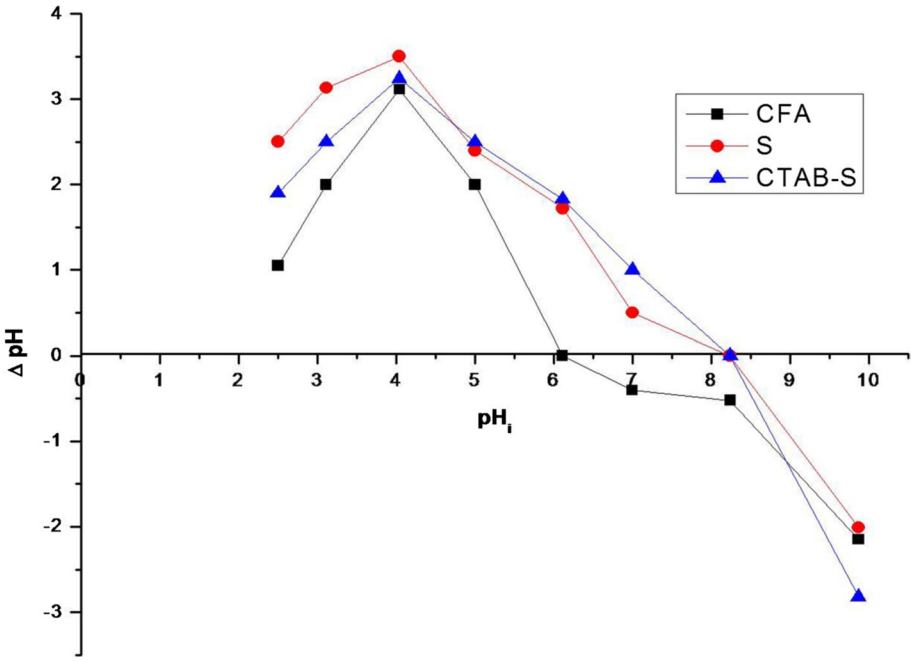

Fig. 6 Optimization of pH_{pzc} using pH drift method

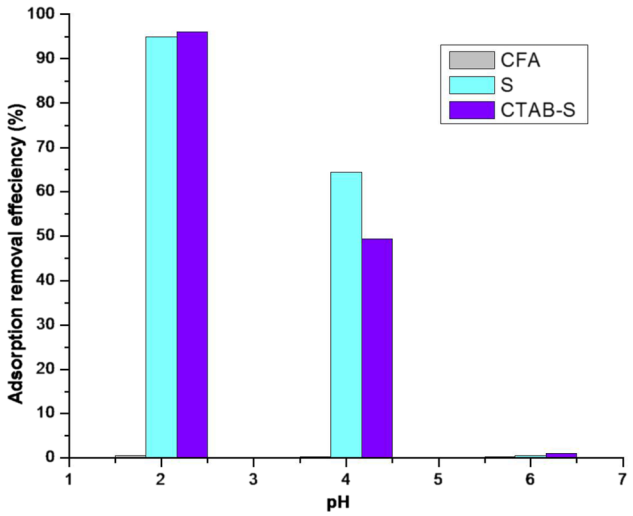

Fig. 7 Effect of pH on the removal efficiency of CR dye

pH_{pzc} determination of treated CFA and their derived-sodalite adsorbents are given in Fig. 6. As demonstrated in this figure, the value of pH_{PZC} for CFA increased from 6.11 to 8.24 for both prepared samples; S and CTAB-S, respectively. Hence, the prepared sodalite samples have predominant basic sites of negatively charged sites and thus can favor the adsorption of cation species. In general terms, pre- and posttreatments with or without CTAB to produce sodalite crystals led to an increase in the development of oxygen functional groups that have been examined by FTIR analysis (OH, Si–O–Al, Si–O–Si), and thus the obtained adsorbents are more attractive to cationic charged particles.

Indeed, the studied dye is anionic, and it bears negative charges that cause repulsion forces with the presented negative charges on the surface of the prepared adsorbents. However, the samples exhibited efficient removal of CR dye in an acidic medium owing to the protonation of Si–O and Si–OH to form positive charges on the sodalite surface, thereby attracting CR dye with negative charges by electrostatic forces as shown in the effect of pH study. This result is in accord with the reported results (Harja et al. 2022) on the adsorption of CR dye onto fly ash, with a maximal adsorption capacity of 22.1 mg/g as a result of surface adsorption (i.e., physisorption).

Adsorption studies

Effect of pH on CR uptake

Influence of pH must be conducted to establish the suitable pH that will facilitate the adsorption isotherms (Yaneva and Georgieva 2012). The percentage of dye adsorption at different pHs (2, 4, and 6) at an initial dye concentration of 40 mg/L is shown in Fig. 7. The measurement was done at a wavelength of 495 nm for pH of 6, at 567 nm for pH of 4 and at 576 nm for pH of 2 (Zhou et al. 2011). Due

to CR dye is a dipolar molecular dye with an isoelectric point of 3, its molecular structure is mostly negative at pH values higher than 3. CR solution color has also been seen to shift from red to dark blue when pH drops. Based on its color fluctuations with pH, the ionic character of CR molecules appear to rely on the pH medium (Purkait et al. 2007). Most of the CFA-derived samples contain oxygen groups on the surface such as O–H and Si–O–Si, Si–OH groups. According to their pH_{ZPC}, i.e., 6.11 for CFA and 8.24 for both prepared samples, the predominant functional groups pose negative charges, whereas at acidic pH these charges became a positive. Hence, the CR dye adsorption on the surface of negatively charges at basic pH is low that is due to the decrease of positive active sites. Inversely, the CR dye adsorption became higher at acidic pH. Hence, its adsorption on the prepared sample surface is substantially higher

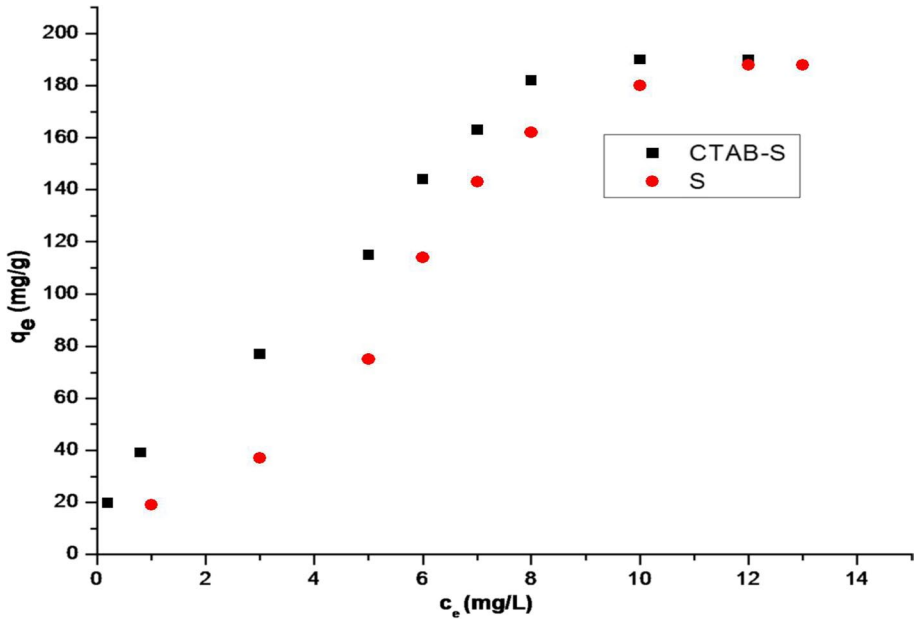

Fig. 8 Adsorption isotherm plateau of prepared samples toward CR dye removal

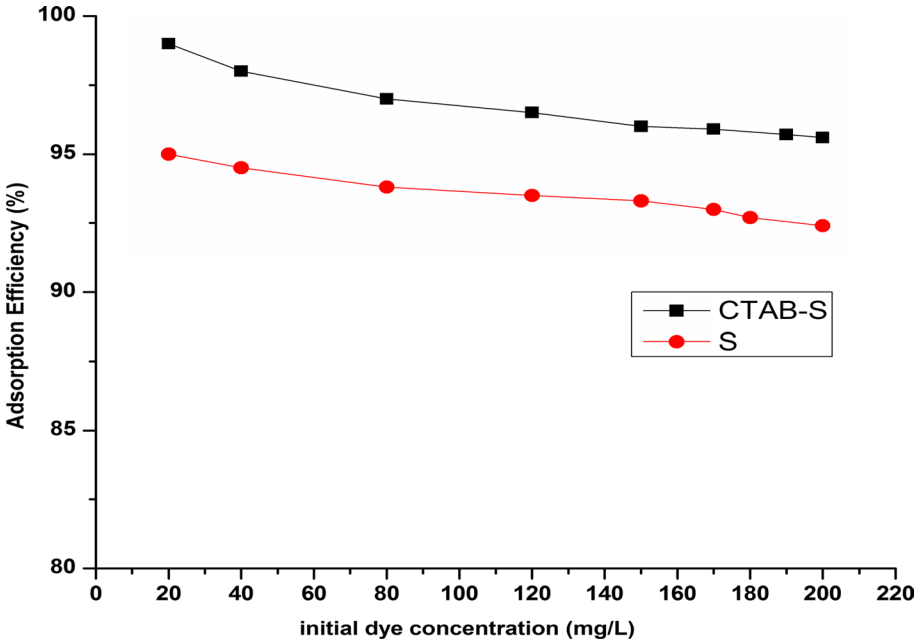

Fig. 9 Removal efficiency at different initial dye concentrations (pH = 2)

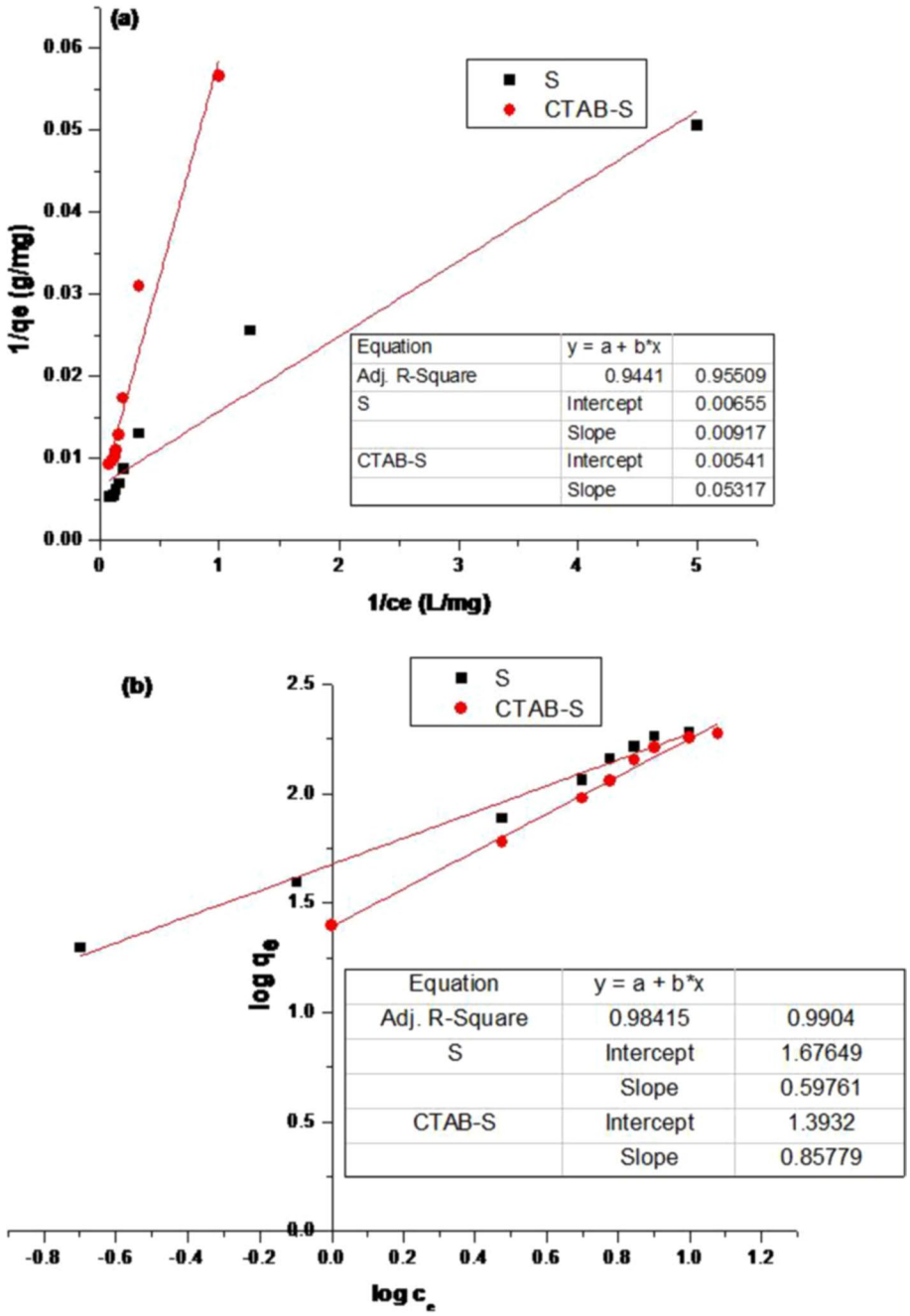

Fig. 10 Linear Plots of **a** Langmuir and **b** Freundlich isotherm models for prepared samples

Table 2 Parameters of Langmuir and Freundlich approaches

Specimens	Langmuir approach				Freundlich approach		
	Q_{max} (mg/g)	k_L (L/mg)	R_L	R^2	k_F ((mg/g) (L/mg))	1/*n*	R^2
S	152.7	0.7	0.012	0.9441	47.5	0.61	0.9845
CTAB-S	184.8	0.1	0.08	0.9551	24.7	0.86	0.9904

at acidic pH (Purkait et al. 2007). As seen in Fig. 7, at pH 2, the percentage of adsorption is the highest (over 90%) at concentration of 40 mg/L of the CR dye. These findings assert that the adsorption process could be explained via electrostatic forces including Van der Waals and H-bonding interactions. Thus, at acidic pH less than 4, the negatively charged sites (Si–O^-) silanol groups on prepared samples become more protonated and form positively groups like Si–OH^{+2}, making them are more appropriate to uptake anionic CR molecules through the electrostatic attraction. Consequently, the adsorption efficiency of CR on adsorbent is enhanced. As pH increases to 6.0, the adsorbent surface turns into negatively charged totally, so the adsorption efficiency substantially decreases. Therefore, the equilibrium adsorption experiments were carried out at optimum pH of 2 and temperature 25 ℃.

Effect of initial dye concentration

Adsorbent and adsorbate equilibrium relationship is often described by an adsorption isotherm. Figure 8 depicts the equilibrium adsorption of CR dye onto the prepared samples. Figure 9 represents the effects of initial CR concentrations (20–200 mg/L) on the percentage of dye removal (pH = 2) at 25 ℃ by CFA-derived samples. At low initial concentrations, the sample of CTAB-S represents higher removal efficiency toward CR dye than S sample. However with increasing the initial concentration, the removal pathway for CR dye by both samples shifted toward the low values but still high by CTAB-S.

Langmuir and Freundlich isotherms study

To identify the kind of interaction between the dye solution and produced adsorbents, equilibrium analysis has been carried out by applying the well-known Langmuir and Freundlich isotherm models. In Fig. 10, both isotherms are shown. The correlation coefficients (R^2) which were calculated from fitting the experimental adsorption equilibrium for both adsorption isotherms are summarized in Table 2. It was found from the values of R^2 that the adsorption of CR over adsorbents was fitted better by Freundlich isotherm, showing the heterogeneity of the surface. Additionally, the values of "n" were greater than unity. This indicates that the CR adsorption onto the samples was successful. From Langmuir isotherm, R_L values were lower than 1 showing that the dye was adsorbed favorably. The calculated maximum adsorption capacity toward CR dye was higher by CTAB-S than that by S (i.e., 152.7 for S and 184.8 mg/g for CTAB-S, respectively) and other adsorbents as listed in Table 3.

Effect of agitation time on adsorption kinetic modeling

The types of physical and/or chemical adsorption interactions (chemical reaction, diffusion control, or mass transfer) that take place between adsorbents and adsorbed species can be described by kinetic adsorption studies (Ghaedi et al. 2012). The impact of contact time on the adsorption of CR dye at two different concentrations (40 and 120 mg/L) was investigated. The plots for CR dynamic studies are shown in Figs. 11, 12, and 13. Table 4 comprises the practically and theoretically estimated adsorption capacity (q_e) as well as

Table 3 Reported maximum adsorption capacities (Q_{max}, mg/g) in the literature for CR dye adsorption and studied specimens

Specimens	Q_{max} (mg/g)	References
S	152.7	This work
CTAB-S	184.8	This work
Activated carbon (Commercial grade)	0.6	Mall et al. (2005)
Activated carbon (Laboratory grade)	1.8	Mall et al. (2005)
Zeolite [Z]	9.23	Dryaz et al. (2021)
Zeolite/algae composite [ZPG]	12.25	Dryaz et al. (2021)
Bagasse fly ash	11.8	Mall et al. (2005)
Fly ash	22	Harja et al. (2022)
Activated carbon	15.8	Basava Rao and Ram Mohan Rao (2006)
Bentonite/zeolite-NaP composite	46	Shaban et al. (2018)
Natural zeolites modified with N,N-dimethyl dehydroabietylamine oxide	69.5	Liu et al. (2014)
Coal-based mesoporous activated carbon	52–189	Lorenc-Grabowska and Gryglewicz (2007)
Hierarchical $Ni(OH)_2$ and NiOnanosheets	40–152	Cheng et al. (2011)
Synthesized zeolites from fly ash [ZS1, ZS2, ZS3, ZS4, ZS5, ZS6, ZS7, CZX]	110–162	Sivalingam and Sen (2018)

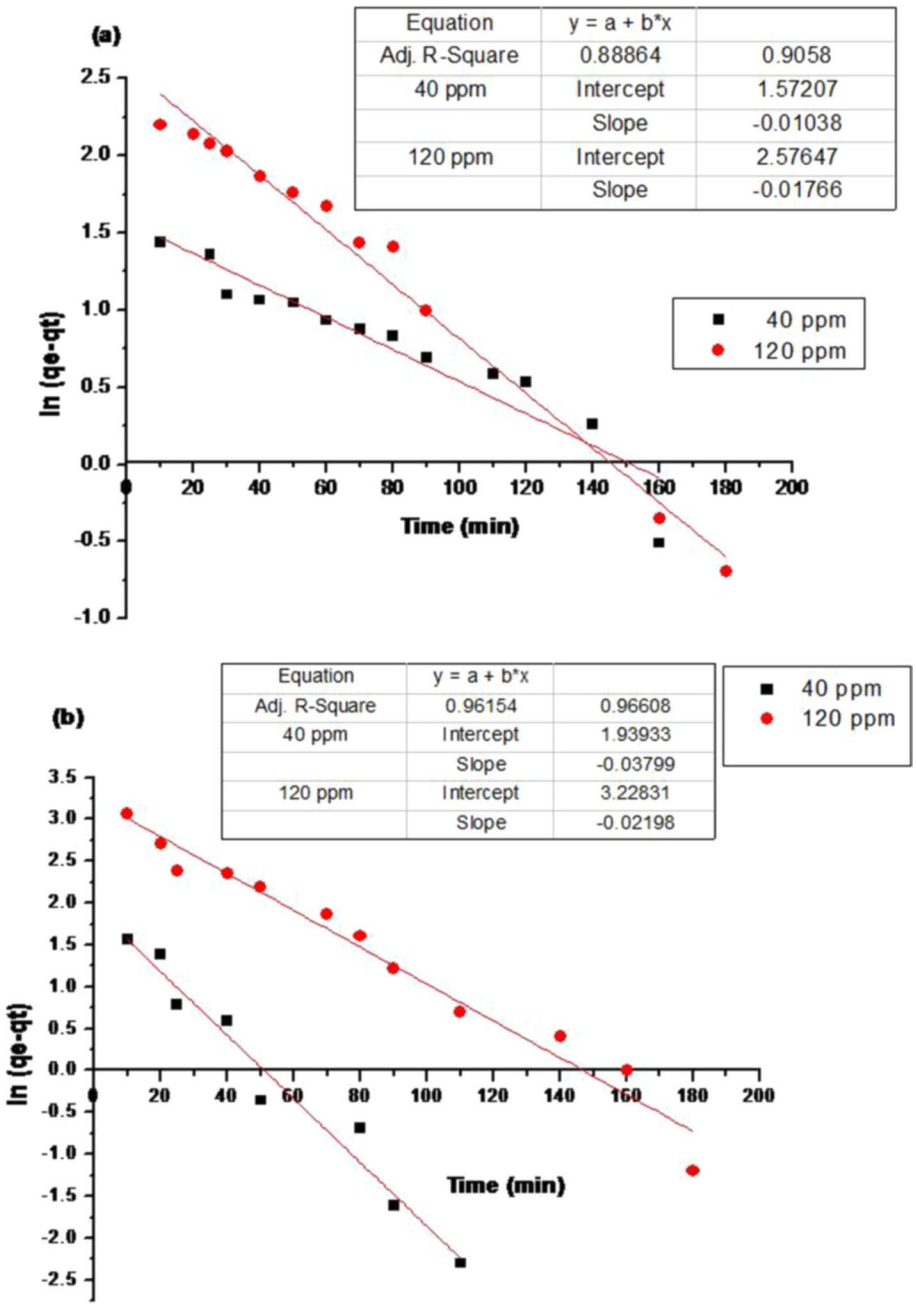

Fig. 11 Pseudo first-order kinetics for prepared CFA-derived silicates; **a** S and **b** CTAB-S

values of k_1, k_2, and R^2. The plots display that the removal of CR dye was significantly rose in the beginning, and the amount of uptaking CR dye still continuously rose as the contact duration grew.

Pseudo first- and second-order kinetic equations

Figure 11 states that the relation between initial dye concentration and rate of adsorption is not linear for pseudo-first order kinetic model reflecting that pore diffusion restricts the adsorption mechanism (Santhi et al. 2010). Furthermore, the majority of the adsorption data in Table 4 have low correlation values (R^2), implying that theoretical and experimental adsorption capabilities vary at equilibrium. Therefore, the reaction mechanism is not a pseudo-first-order kinetic model.

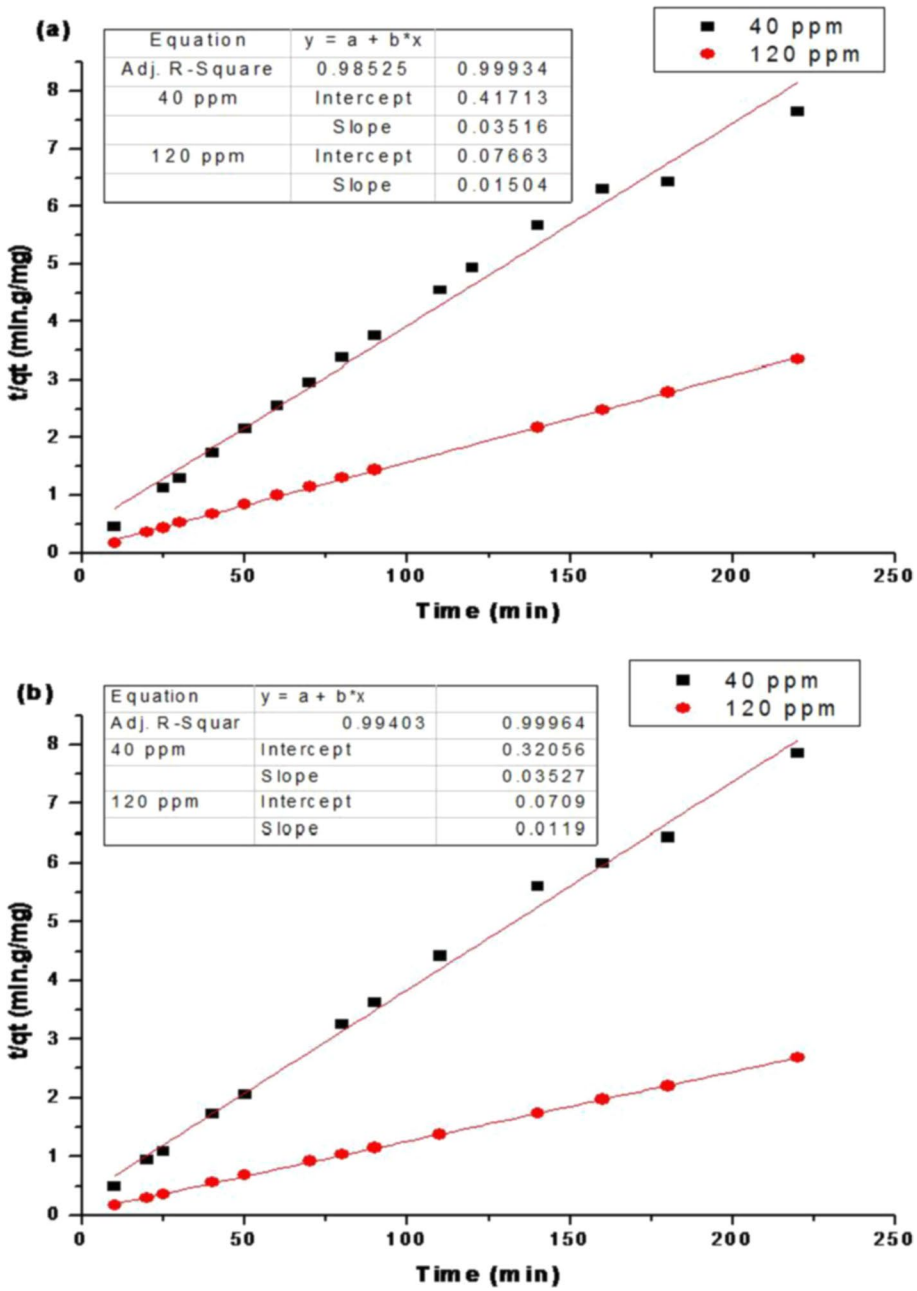

Fig. 12 Pseudo second-order kinetics for prepared CFA-derived silicates; **a** S and **b** CTAB-S

It can be seen that pseudo-second-order kinetic model is relevant because a linear connection between t/q_t, and t is seen on the plot. From the intercept and slope of the plots of t/q_t versus t, values of k_2 and equilibrium adsorption capacity (q_e) were derived, respectively (Fig. 12). The q_e values of the two studied initial concentrations of CR dye were approximated by the linear plots between experimental and estimated values (Table 4). Accordingly, the pseudo-second-order kinetic model has high correlation values (R^2) larger than 0.96 for the adsorption of CR dye. As a result, the pseudo-second-order kinetic model for the CFA-derived sodalite is the better to simulate the adsorption kinetics for CR dye. It can be claimed from these findings that the CR dye adsorption contains a chemical process also as well as physico-adsorption stage based on pH results.

Intra-particular diffusion equation

The possibility of intra-particular diffusion mechanism was assessed utilizing the intraparticle diffusion model.

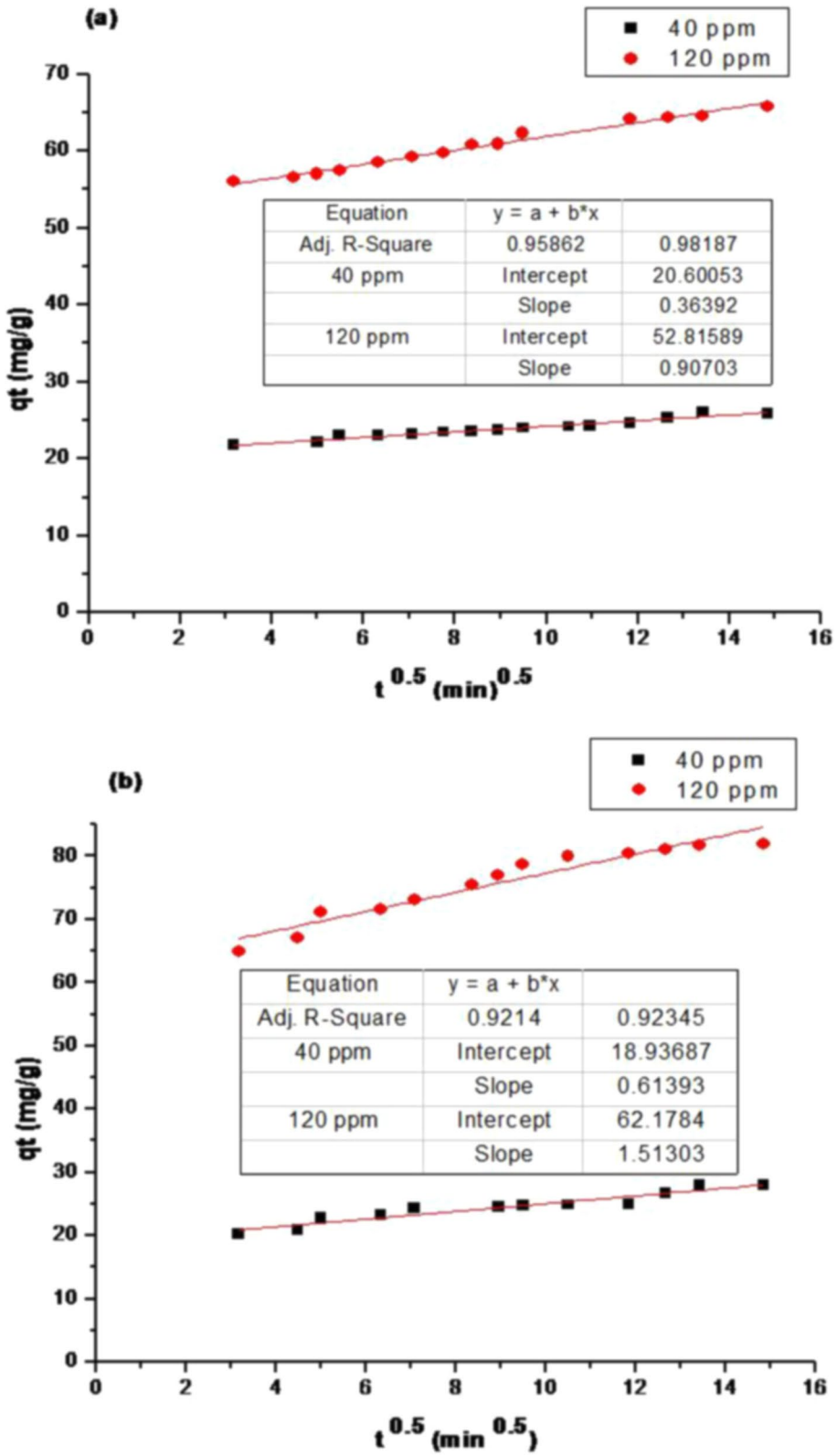

Fig. 13 Intra-particle diffusion for prepared CFA-derived silicates; **a** S and **b** CTAB-S

Table 4 Kinetic constants for CR dye removal by prepared CFA-derived samples

Kinetic parameters	q_e (exp) (mg/g)	K_1 (min^{-1})	q_e (mg/g)	R^2	K_2 (min^{-1})	q_e (mg/g)	R^2
S							
40 ppm	26	0.01	4.8	0.888	0.003	28.5	0.985
120 ppm	65	0.02	13.2	0.905	0.0029	66.5	0.999
CTAB-S							
40 ppm	24	0.04	7.0	0.961	0.004	28.3	0.994
120 ppm	81.5	0.02	25.2	0.966	0.002	84	0.999

Intra-particle diffusion parameters	K_{id} (mg/g.min0.5)	C	R^2
S			
40 ppm	0.40	20.6	20.6
120 ppm	0.91	50.8	0.981
CTAB-S			
40 ppm	0.61	18.9	0.921
120 ppm	1.5	62.2	0.923

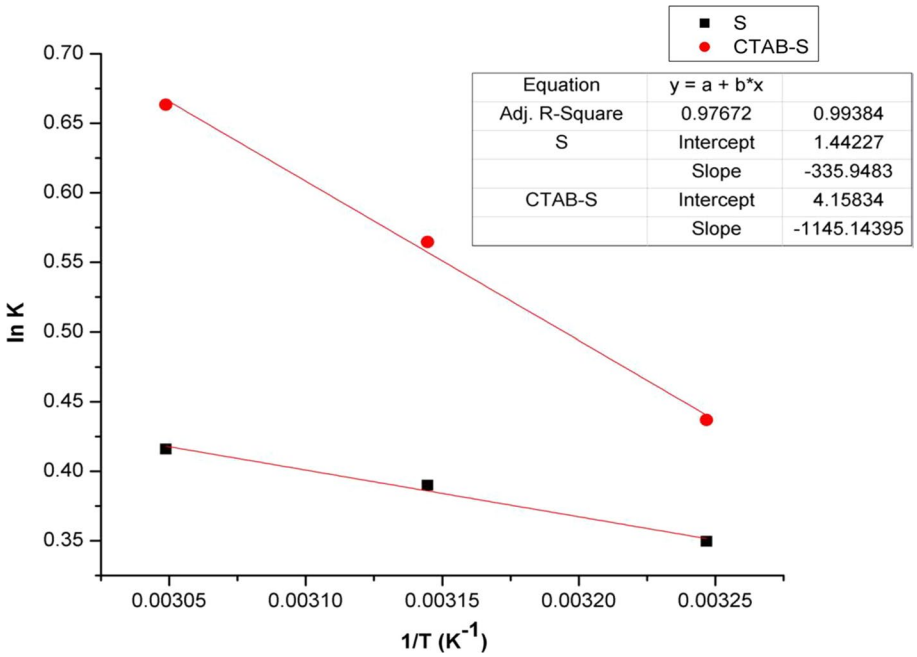

Fig. 14 Vant Hoff equation for adsorption attainment of CR dye on prepared CFA-based silicate samples

Table 5 Thermodynamic specifications for the adsorption of CR dye on prepared samples

Thermodynamic Parameters	Temperature (K)	S	CTAB-S
ΔG^o (kJ/mol)	308	−0.9	−1.2
	318	−1.02	−1.5
	328	−1.14	−1.85
ΔH^o (kJ/mol)		+2.8	+9.5
ΔS^o (J/mol. K)		+12	+35

This model represents a relationship between values of q_t correlated linearly with values of $t^{1/2}$ (see Fig. 13); in order to calculate the rate constant K_{id} which probed from the slope (Table 4). If the plot is a linear and crosses through the origin, thus the sole rate-limiting mechanism is the intraparticle diffusion (Bulut et al. 2008). If such a line does not cross through the origin, an intraparticle diffusion occurs in the adsorption process followed by additional mechanisms such as a complexation, pore diffusion, or/

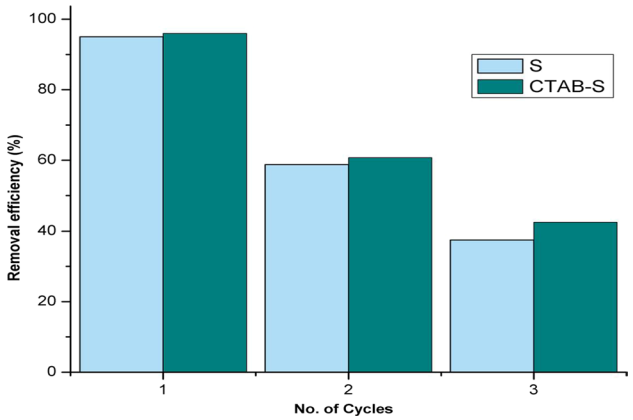

Fig. 15 Reusability of CFA-based silicates for removing CR dye

and ion exchange process (Crini et al. 2007). The values of intercept (*C*) provide also data about the thickness of the boundary layer. Consequently, resistance to external mass transfer increases as *C* value enhances with increasing dye concentration, indicating that the thickness of the boundary layer is increased (Kavitha and Namasivayam 2007) as shown in Table 4. The R^2 values for this model were found to be between 0.921 and 0.982 emphasizing that the CR adsorption onto these new adsorbents can follow the intraparticle diffusion in the first stage and then followed by another mechanism such as pore diffusion and ion exchange processes.

Thermodynamic studies

Various temperatures (308, 318, and 328 K) were used to explore the adsorption of CR dye onto CFA-based adsorbents. Figure 14 and Table 5 present the findings. The positive results of ΔH° (2.8 and 9.5 kJ/mol) for S and CTAB-S, respectively, confirmed that the interaction of the CR dye adsorbed onto the CFA-based adsorbents was endothermic in nature (Mohamed et al. 2019). Additionally, negative values of ΔG° at the specified temperatures demonstrated that the CR dye adsorbed onto the adsorbents is a spontaneous process (Al-Harby et al. 2021). The enhanced randomness at the boundary between the adsorbent and adsorbate solution throughout CR dye adsorption was evidenced by the positive value of ΔS° (Tahira et al. 2019). Accordingly, the dye molecule got additional entropy as a result of the adsorbed solvent molecule being displaced, which ultimately led to an increase in the randomness (Al-Harby et al. 2021).

Reusability study

Reusability studies on the prepared sodalite-based adsorbents were carried out as a key factor in cost-effective water treatment. The previously used adsorbents were reactivated by washing them in double-distilled water for several times. The final product was then dried at 80 ℃ and applied once more for upto three subsequent cycles of decontaminating CR dye (40 mg/L) at 25 ℃. Figure 15 displays the results of dye adsorption. It was disclosed that when the number of cycles increased, the CR dye adsorption became less effective. Even after the third cycle, "CTAB-S" sample still displayed an improved adsorption capacity compared to prepared "S." As a result, it was concluded that sodalite-based adsorbents are suitable recyclable adsorbents for the removal of CR dye from aqueous media.

Conclusion

The present study shows that the CFA, a by-product of power stations, can be converted successfully to sodalite zeolitic structure adsorbents via post calcination at 550 ℃ after forming sodium-aluminum silicates. Adsorption outcomes of anionic CR dye significantly dependent on variable parameters such as pH, contact time and initial dye concentration. The adsorption is enhanced as a result of electrostatic forces including Van der Waals and H – bonding interactions at acidic pHs. Equilibrium adsorption data can be followed preferably by Freundlich isotherm. The maximum adsorption capacity of CR dye has been counted from Langmuir model to be 152.7 and 184.8 mg/g over S and CTAB-S, respectively. Kinetic data followed a pseudo-second order and the adsorption process was controlled by a chemical adsorption. An intraparticle diffusion mechanism on the surface of both samples was not occurred alone but also other mechanisms such as pore diffusion and ion exchange processes happened. Finally, the CR dye adsorption is influenced by physicochemical mechanisms, according to pH and kinetic data. As a result, the S and CTAB-S sodalite samples produced provide an efficient surface for extracting the CR dye from aqueous solutions.

Acknowledgements Authors are thankful to the National Research Center, Egypt, for supporting this work with technical facilities including chemicals and equipment.

Author contributions All the authors contributed equally to this work.

Funding Open access funding provided by The Science, Technology & Innovation Funding Authority (STDF) in cooperation with The Egyptian Knowledge Bank (EKB). The author(s) received no specific financial funding for this work.

Declarations

Conflict of interest The authors declare that they have no known competing financial interests or personal relationships that could have appeared to influence the work reported in this paper.

References

Aboelenin RMM, Fathy NA, Farag HK, Sherief MA (2017) Preparation, characterization and catalytic performance of mesoporous silicates derived from natural diatomite: comparative studies. J Water Process Eng 19:112–119. https://doi.org/10.1016/j.jwpe.2017.07.017

Ahmad MA, Herawan SG, Yusof AA (2014) Equilibrium, kinetics, and thermodynamics of remazol brilliant blue r dye adsorption onto activated carbon prepared from pinang frond. ISRN Mech Eng 2014:1–7. https://doi.org/10.1155/2014/184265

Ahmadpour J, Taghizadeh M (2015) Catalytic conversion of methanol to propylene over high-silica mesoporous ZSM-5 zeolites prepared by different combinations of mesogenous templates. J Nat Gas Sci Eng 23:184–194. https://doi.org/10.1016/j.jngse.2015.01.035

Al-Harby NF, Albahly EF, Mohamed NA (2021) Kinetics, isotherm and thermodynamic studies for efficient adsorption of Congo red dye from aqueous solution onto novel cyanoguanidine-modified chitosan adsorbent. Polymers (basel) 13:1–32. https://doi.org/10.3390/polym13244446

Alterary S, Marei NH (2020) The impact of coal fly ash purification on its antibacterial activity. Minerals 10:1–14. https://doi.org/10.3390/min10111002

Amani S, Garmarudi AB, Khanmohammadi M, Yaripour F (2018) Application of diffuse reflectance near-infrared spectrometry and chemometrics in characterization of micro and mesoporous ZSM-5 zeolites. RSC Adv 8:34830–34837. https://doi.org/10.1039/c8ra03244k

Bardez I, Campayo L, Rigaud D, et al (2008) Investigation of sodalites for conditioning halide salts (NaCl and NaI): comparison of two synthesis routes. ATALANTE, pp. 1–7

Basava Rao VV, Ram Mohan Rao S (2006) Adsorption studies on treatment of textile dyeing industrial effluent by flyash. Chem Eng J 116:77–84. https://doi.org/10.1016/j.cej.2005.09.029

Bulut E, Özacar M, Şengil IA (2008) Equilibrium and kinetic data and process design for adsorption of Congo red onto bentonite. J Hazard Mater 154:613–622. https://doi.org/10.1016/j.jhazmat.2007.10.071

Cao XQ, Wang X, Chen M et al (2021) Synthesis of nanoscale zeolitic imidazolate framework-8 (ZIF-8) using reverse micro-emulsion for Congo red adsorption. Sep Purif Technol 260:1–43. https://doi.org/10.1016/j.seppur.2020.118062

Cheng B, Le Y, Cai W, Yu J (2011) Synthesis of hierarchical Ni(OH)2 and NiO nanosheets and their adsorption kinetics and isotherms to Congo red in water. J Hazard Mater 185:889–897. https://doi.org/10.1016/j.jhazmat.2010.09.104

Crini G, Peindy HN, Gimbert F, Robert C (2007) Removal of C.I. basic green 4 (Malachite green) from aqueous solutions by adsorption using cyclodextrin-based adsorbent: kinetic and equilibrium studies. Sep Purif Technol 53:97–110. https://doi.org/10.1016/j.seppur.2006.06.018

Delle Site A (2001) Factors affecting sorption of organic compounds in natural sorbent/water systems and sorption coefficients for selected pollutants. a review. J Phys Chem Ref Data 30:187–439. https://doi.org/10.1063/1.1347984

Dryaz AR, Shaban M, AlMohamadi H et al (2021) Design, characterization, and adsorption properties of Padina gymnospora/zeolite nanocomposite for Congo red dye removal from wastewater. Sci Rep 11:1–16. https://doi.org/10.1038/s41598-021-00025-y

El-Sherif IY, Fathy NA (2013) Modification of adsorptive properties of bagasse fly ash for uptaking cadmium from aqueous solution. Environ Res Eng Manag 64:19–28. https://doi.org/10.5755/j01.erem.64.2.3576

Esaifan M, Warr LN, Grathoff G et al (2019) Synthesis of hydroxy-sodalite/cancrinite zeolites from calcite-bearing kaolin for the removal of heavy metal ions in aqueous media. Minerals 9:1–13. https://doi.org/10.3390/min9080484

Foo KY, Hameed BH (2010) Insights into the modeling of adsorption isotherm systems. Chem Eng J 156:2–10. https://doi.org/10.1016/j.cej.2009.09.013

Freundlich HMF (1906) Over the adsorption in solution. J Phys Chem 57:385–471

Ghaedi M, Biyareh MN, Kokhdan SN et al (2012) Comparison of the efficiency of palladium and silver nanoparticles loaded on activated carbon and zinc oxide nanorods loaded on activated carbon as new adsorbents for removal of Congo red from aqueous solution: kinetic and isotherm study. Mater Sci Eng C 32:725–734. https://doi.org/10.1016/j.msec.2012.01.015

Golbad S, Khoshnoud P, Abu-Zahra N (2017) Hydrothermal synthesis of hydroxy sodalite from fly ash for the removal of lead ions from water. Int J Environ Sci Technol 14:135–142. https://doi.org/10.1007/s13762-016-1133-x

Günther C, Richter H, Voigt I et al (2015) Synthesis and characterization of a sulfur containing hydroxy sodalite without sulfur radicals. Microporous Mesoporous Mater 214:1–7. https://doi.org/10.1016/j.micromeso.2015.04.024

Harja M, Buema G, Bucur D (2022) Recent advances in removal of Congo red dye by adsorption using an industrial waste. Sci Rep 12:1–19. https://doi.org/10.1038/s41598-022-10093-3

Ho YS, Chiang CC (2001) Sorption studies of acid dye by mixed sorbents. Adsorption 7:139–147. https://doi.org/10.1023/A:1011652224816

Jiang C, Fu B, Cai H, Cai T (2016) Efficient adsorptive removal of Congo red from aqueous solution by synthesized zeolitic imidazolate framework-8. Chem Speciat Bioavailab 28:199–208. https://doi.org/10.1080/09542299.2016.1224983

Kavitha D, Namasivayam C (2007) Experimental and kinetic studies on methylene blue adsorption by coir pith carbon. Bioresour Technol 98:14–21. https://doi.org/10.1016/j.biortech.2005.12.008

Khattab RM, Sadek HEH, Abo-almaged HH (2018) Mullite-cobalt (II, III) oxide system: preparation of ceramic pigment using

recycling of fly ash. Silicon 10:1487–1495. https://doi.org/10.1007/s12633-017-9630-1
Kumar P, Mal N, Oumi Y et al (2001) Mesoporous materials prepared using coal fly ash as the silicon and aluminium source. J Mater Chem 11:3285–3290. https://doi.org/10.1039/b104810b
Lagergren S (1898) Zur Theorie der Sogenannten Adsorption Gelöster Stoffe, Kungliga Svenska Vetenskapsakademiens. Handlingar 24:1–39
Langmuir I (1916) The constitution and fundamental properties of solids and liquids. Part I solids. J Am Chem Soc 38:2221–2295. https://doi.org/10.1021/ja02268a002
Liu S, Ding Y, Li P et al (2014) Adsorption of the anionic dye Congo red from aqueous solution onto natural zeolites modified with N, N-dimethyl dehydroabietylamine oxide. Chem Eng J 248:135–144. https://doi.org/10.1016/j.cej.2014.03.026
Lorenc-Grabowska E, Gryglewicz G (2007) Adsorption characteristics of Congo red on coal-based mesoporous activated carbon. Dye Pigment 74:34–40. https://doi.org/10.1016/j.dyepig.2006.01.027
Luo J, Zhang H, Yang J (2016) Hydrothermal synthesis of sodalite on alkali-activated coal fly ash for removal of lead ions. Procedia Environ Sci 31:605–614. https://doi.org/10.1016/j.proenv.2016.02.105
Makgabutlane B, Nthunya LN, Nxumalo EN et al (2020) Microwave irradiation-assisted synthesis of zeolites from coal fly ash: an optimization study for a sustainable and efficient production process. ACS Omega 5:25000–25008. https://doi.org/10.1021/acsomega.0c00931
Mall ID, Srivastava VC, Agarwal NK, Mishra IM (2005) Removal of congo red from aqueous solution by bagasse fly ash and activated carbon: kinetic study and equilibrium isotherm analyses. Chemosphere 61:492–501. https://doi.org/10.1016/j.chemosphere.2005.03.065
Mohamed NA, Al-harby NF, Almarshed MS (2019) Enhancement of adsorption of Congo red dye onto novel antimicrobial trimellitic anhydride isothiocyanate—cross-linked chitosan hydrogels. Polym Bull. https://doi.org/10.1007/s00289-019-03058-6
Mohan D, Chander S (2001) Single component and multi-component adsorption of metal ions by activated carbons. Colloids Surf A Physicochem Eng Asp 177:183–196. https://doi.org/10.1016/S0927-7757(00)00670-1
Mozgawa W, Król M, Dyczek J, Deja J (2014) Investigation of the coal fly ashes using IR spectroscopy. Spectrochim Acta Part A Mol Biomol Spectrosc 132:889–894. https://doi.org/10.1016/j.saa.2014.05.052
Mucsi G, Molnár Z, Kumar S (2014) Geopolymerisation of mechanically activated lignite and brown coal fly ash. In: Proceedings of the 8th international conference on mechanochemistry and mechanical alloying, INCOME 2014, pp. 994–998
Münzer S, Caro J, Behrens P (2008) Preparation and characterization of sodium-free nanocrystalline sodalite. Microporous Mesoporous Mater 110:3–10. https://doi.org/10.1016/j.micromeso.2007.07.040
Musyoka NM, Missengue R, Kusisakana M, Petrik LF (2014) Conversion of South African clays into high quality zeolites. Appl Clay Sci 97–98:182–186. https://doi.org/10.1016/j.clay.2014.05.026
Nabavi MS, Mohammadi T, Kazemimoghadam M (2014) Hydrothermal synthesis of hydroxy sodalite zeolite membrane: separation of H2/CH4. Ceram Int 40:5889–5896. https://doi.org/10.1016/j.ceramint.2013.11.033
Ojha K, Pradhan NC, Samanta AN (2004) Zeolite from fly ash: synthesis and characterization. Bull Mater Sci 27:555–564. https://doi.org/10.1007/BF02707285
Perrot P (1998) A to Z of thermodynamics. Oxford Univ Press
Purkait MK, Maiti A, DasGupta S, De S (2007) Removal of Congo red using activated carbon and its regeneration. J Hazard Mater 145:287–295. https://doi.org/10.1016/j.jhazmat.2006.11.021
Purnawira B, Purwaningsih H, Ervianto Y et al (2019) Synthesis and characterization of mesoporous silica nanoparticles (MSNp) MCM 41 from natural waste rice husk. IOP Conf Ser Mater Sci Eng. https://doi.org/10.1088/1757-899X/541/1/012018
Rangabhashiyam S, Anu N, GiriNandagopal MS, Selvaraju N (2014) Relevance of isotherm models in biosorption of pollutants by agricultural byproducts. J Environ Chem Eng 2:398–414. https://doi.org/10.1016/j.jece.2014.01.014
Ravikumar RVSSN, Chandrasekhar AV, Yamauchi J et al (2005) Tetrahedral site of iron in natural mineral sodalite. Radiat Eff Defects Solids 160:109–115. https://doi.org/10.1080/10420150500132364
Santhi T, Manonmani S, Smitha T (2010) Kinetics and isotherm studies on cationic dyes adsorption onto annona squmosa seed activated carbon. Int J Eng Sci Technol 2:287–295
Shaban M, Abukhadra MR, Shahien MG, Ibrahim SS (2018) Novel bentonite/zeolite-NaP composite efficiently removes methylene blue and Congo red dyes. Environ Chem Lett 16:275–280. https://doi.org/10.1007/s10311-017-0658-7
Shabani JM, Babajide O, Oyekola O, Petrik L (2019) Synthesis of hydroxy sodalite from coal fly ash for biodiesel production from waste-derived maggot oil. Catalysts 9:1–14. https://doi.org/10.3390/catal9121052
Shumba M, Chigondo M, Guyo U et al (2011) Synthesis of zeolites and their applications in heavy metals removal : a review. IRACST Eng Sci Technol An Int J 30:1–7
Singh S, Jain A, Rao Tiwari K et al (2019) Synthesis and characterization of zeolite linde W and its application as adsorbent for pesticide. Int J Mater Sci 14:17–30. https://doi.org/10.24941/ijcr.33245.11.2018
Sivalingam S, Sen S (2018) Rapid ultrasound assisted hydrothermal synthesis of highly pure nanozeolite X from fly ash for efficient treatment of industrial effluent. Chemosphere 210:1–20. https://doi.org/10.1016/j.chemosphere.2018.07.091
Sotomayor FJ, Cychosz KA, Thommes M (2018) Characterization of micro/mesoporous materials by physisorption: concepts and case studies. Acc Mater Surf Res 3:34–50
Suriyana RN, Nithin KVK, Bernando E (2009) Mullite glass ceramics production from coal ash and alumina by high temperature plasma. J Non-Oxide Glas 1:247–260
Tahira I, Aslam Z, Abbas A, Monim- M (2019) Adsorptive removal of acidic dye onto grafted chitosan: a plausible grafting and adsorption mechanism. Int J Biol Macromol. https://doi.org/10.1016/j.ijbiomac.2019.06.173
Taufiq A, Hidayat P, Hidayat A (2018) Modified coal fly ash as low cost adsorbent for removal reactive dyes from batik industry. MATEC Web Conf 154:1–5. https://doi.org/10.1051/matecconf/201815401037
Thanh Tu NT, Thien TV, Du PD et al (2018) Adsorptive removal of Congo red from aqueous solution using zeolitic imidazolate framework-67. J Environ Chem Eng 6:2269–2280. https://doi.org/10.1016/j.jece.2018.03.031

Vimonses V, Jin B, Chow CWK (2010) Insight into removal kinetic and mechanisms of anionic dye by calcined clay materials and lime. J Hazard Mater 177:420–427. https://doi.org/10.1016/j.jhazmat.2009.12.049

Weber TW, Chakravorti RK (1974) Pore and solid diffusion models for fixed-bed adsorbers. Aiche J 20:228–238

Weber WJ, Morris JC (1963) Kinetics of adsorption on carbon from solution. J Sanit Eng Div Am Soc Civ Eng 89:31–60

Yadav VK, Fulekar MH (2019) Green synthesis and characterization of amorphous silica nanoparticles from fly ash. Mater Today Proc 18:4351–4359. https://doi.org/10.1016/j.matpr.2019.07.395

Yaneva ZL, Georgieva NV (2012) Insights into Congo red adsorption on agro-industrial materials—spectral, equilibrium, kinetic, thermodynamic, dynamic and desorption studies. Rev Int Rev Chem Eng 4:127–146

Zhao D, Wan Y, Zhou W (2013) Ordered mesoporous materials. Markono Print Media Pte Ltd, Singapore

Zhou Q, Xie C, Gong W et al (2011) Comments on the method of using maximum absorption wavelength to calculate Congo Red solution concentration. Elsevier